CHEMISTRY OF MATERIALS
Article

Chem. Mater. **2010,** *22,* 6459–6466 6459
DOI:10.1021/cm102827y

Synthesis and Characterization of Zwitterionic SBA-15 Nanostructured Materials

Montserrat Colilla,[†,‡] Isabel Izquierdo-Barba,[†,‡] Sandra Sánchez-Salcedo,[†,‡] José L. G. Fierro,[§] José L. Hueso,[‡] and María Vallet-Regí*[,†,‡]

[†]*Dpto. Química Inorgánica y Bioinorgánica, Facultad de Farmacia, Universidad Complutense de Madrid, Plaza Ramón y Cajal s/n, 28040 Madrid, Spain,* [‡]*Networking Research Center on Bioengineering, Biomaterials and Nanomedicine* (*CIBER-BBN*), *Madrid, Spain, and* [§]*Instituto de Catálisis y Petroleoquímica, CSIC, Cantoblanco, 28049 Madrid, Spain*

Received September 30, 2010

The synthesis and characterization of novel SBA-15 nanostructured ceramics featuring zwitterionic surfaces have been carried out. The co-condensation route has been employed to bifunctionalize SBA-15 with amine and carboxylic acid groups. The functionalization process following a one-step route does not affect the mesostructural order of SBA-15, as confirmed by XRD and TEM, originating mesoporous matrices with outstanding features suitable for purposes that require host matrices with relatively large mesopores, surface areas, and volumes. The zwitterionic nature of this material has been evidenced by XPS, FTIR, and ζ-potential. Moreover the ultralow-fouling behavior of this zwitterionic ceramic toward the adsorption a model protein has been confirmed. This novel generation of zwitterionic ceramics has great potential application in catalysis, sensing, biotechnology, and biomedicine.

Introduction

The development of materials with high resistance to biofouling adhesion is essential for a wide range of applications in catalysis, sensing, biotechnology, and biomedicine.[1−6] Different approaches have been investigated in an effort to solve this drawback, such the use of hydrophilic surfaces by coating with poly(ethylene glycol) PEG derivates.[7,8] However, these surfaces do not reduce the nonspecific protein adhesion sufficiently to fulfill the ultralow-fouling criterion (< 5 ng/cm^2).[9] Recently, zwitterionic polymers as poly(carboxybetaine methacrylate) (pCBMA) and poly(sulfobetaine methacrylate) (pSBMA) containing quaternary ammonium as positive charge and carboxylate and sulfate as negative charges have been reported as good ultralow-fouling materials.[9]

Ordered mesoporous silicas have been extensively employed in different application fields such as catalysis, sensing, biotechnology, and biomedicine.[10−15] In fact, bifunctionalized mesoporous silicas containing acid and basic groups have been recently reported for electrochemical and catalytic purposes.[16−18] Therefore the design of organic inorganic mesoporous hybrids featuring zwitterionic surfaces with ultralow-fouling capability would represent a very promising next-generation of materials suitable for a wide range of technological applications.

Herein, we report for the first time the one-step synthesis of zwitterionic SBA-15 type mesoporous material containing both COO^- and NH_3^+ groups exhibiting ultralow-fouling capability. The zwitterionic nature of this material was characterized by different physicochemical techniques such as X-ray photoelectron spectroscopy (XPS) and Fourier transform infrared spectroscopy (FTIR) to demonstrate the presence of ion pairs in the hybrid material between the two functions of opposite charge. Therefore, the results here presented demonstrate that XPS is a very powerful tool for the characterization of this type of material. To determine the pH conditions in which the zwitterionic nature of the material surface is preserved in aqueous media, the isoelectric point (IEP) of samples, which is tightly related to the zero point

*Corresponding author: vallet@farm.ucm.es.

(1) Prime, K. L.; Whitesides, G. M. *Science* **1991**, *252*, 1164.
(2) Castner, D. G.; Ratner, B. D. *Surf. Sci.* **2002**, *500*, 28.
(3) Ladd, J.; Zhang, Z.; Chen, S.; Hower, J. C.; Jiang, S. *Biomacromolecules* **2008**, *9*, 1357.
(4) Vaisocherova, H.; Yang, W.; Zhang, Z.; Cao, Z.; Cheng, G.; Piliarik, M.; Homola, J.; Jiang, S. *Anal. Chem.* **2008**, *80*, 7894.
(5) Magin, C. M.; Cooper, S. P.; Brennan, A. B. *Mater. Today* **2010**, *13*, 36.
(6) Ruiz, A.; Mills, C. A.; Valsesia, A.; Martínez, E.; Cecoone, G.; Samitier, J.; Colpo, P.; Rossi, F. *Small* **2009**, *5*, 1133.
(7) Kasemo, B. *Surf. Sci.* **2002**, *500*, 656.
(8) Khoo, X.; Hamilton, P.; O'Toole, G. A.; Snyder, B. D.; Kenan, D. J.; Grinstaff., M. W. *J. Am. Chem. Soc.* **2009**, *131*, 10992.
(9) Jiang, S.; Cao, Z. *Adv. Mater.* **2009**, *21*, 1.
(10) Walcarius, A. *Electroanalysis* **1998**, *10*, 1217.
(11) Scott, B. J.; Wirnsberger, G.; Stucky, G. D. *Chem. Mater.* **2001**, *13*, 3140.
(12) Davis, M. E. *Nature* **2002**, *417*, 813.
(13) Hartmann, M. *Chem. Mater.* **2005**, *17*, 4577.
(14) Kuscheel, A.; Drescher, M.; Kuschel, T.; Polarz, S. *Chem. Mater.* **2010**, *22*, 1472.
(15) Vallet-Regí, M. *J. Int. Med.* **2010**, *267*, 22.
(16) Huh, S.; Chen, H. −T.; Wiench, J. W.; Pruski, M.; Lin, V. S. −Y. *Angew. Chem., Int. Ed.* **2005**, *44*, 1826.
(17) Han, L.; Ruan, J.; Li, Y.; Terasaki, O.; Che., S. *Chem. Mater.* **2007**, *19*, 2860.
(18) Walcarius, A.; Ganesan, V. *Langmuir* **2006**, *22*, 469.

© 2010 American Chemical Society
Published on Web 11/04/2010

Table 1. Different Molar Compositions of the Precursor Sols Used during the Synthesis of the Different Mesoporous Materials

sample	TEOS	APTES	CES	P123	HCl	H_2O
SBA-15	1	0	0	0.017	3.4	208
$SBA15_{APTES}$	0.98	0.02	0	0.017	3.4	208
$SBA15_{CES}$	0.97	0	0.03	0.017	3.4	208
$SBA15_{APTES/CES}$	0.93	0.035	0.035	0.017	3.4	208

charge,[19] was determined by ζ-potential measurements. The effect of the simultaneous presence of carboxylate and ammonium groups in the material surface on nonspecific protein adsorption has been investigated.

Materials and Methods

Synthesis of Functionalized SBA-15 Structures. SBA-15 type silica mesoporous material has been doubly functionalized with amine and carboxylic groups by co-condensation route using 3-aminopropyltriethoxy-silane (APTES, 99% wt., ABCR) together with carboxyethylsilanetriol sodium salt (CES, 25% vol., ABCR). For comparison, pure SBA-15 and SBA-15 type monofunctionalized mesoporous materials with amine or carboxylic acid groups have been also synthesized. Table 1 displays the amount of each reactant employed for the synthesis of the different materials and the adopted nomenclature.

Briefly, 4.0 g of Pluronic P123 (Pluronic P123, BASF) was added to a mixture of 138.0 g of H_2O and 10.3 mL of concentrated HCl (Aldrich, 37% wt.).[20] The solution was moderately stirred for 4 h at 40 °C until total surfactant dissolution. Then, the corresponding amount of tetraethyl orthosilicate (TEOS, 98% wt., Sigma-Aldrich) was added and the appropriate amounts of functionalization agents, APTES and/or CES, were simultaneously added to the solution. Sols were kept at 40 °C during 24 h in sealed glass beakers and subsequently heated at 100 °C for 24 h. The obtained products were filtered, washed with deionized water, and then dried at 50 °C for 12 h in air. Then, the surfactant was removed by extraction using different solvents or mixtures of solvents depending on the functionalization agent employed, as elsewhere described.[17] In the case of pure SBA-15 and $SBA15_{APTES/CES}$ materials, 0.5 g of the as-synthesized material was first refluxed at 80 °C with a THF/HCl (10:1 volume ratio) solution for 15 h. Afterward, the solution was refluxed with an ethanolic solution of ethanolamine (20 vol.%) for another 15 h at 80 °C. A third extraction process with acetone/ether (1:1) was performed to eliminate all the rest of ethanolic solution for 15 h at room temperature. In the case of $SBA15_{CES}$ sample, the surfactant was removed by performing two subsequent extraction cycles using a THF/HCl solution (10:1 volume ratio) at 80 °C for 15 h. The surfactant was extracted in $SBA15_{APTES}$ sample by two extraction cycles with an ethanolic solution of ethanolamine (20 vol.%) at 80 °C for 15 h. In all cases after the extraction processes samples were left to dry into vacuum oven during 24 h to ensure total solvent removal.

Characterization of Materials. The structural characteristics of the resulting materials were determined by powdered X-ray diffraction (XRD) in a Philips X'Pert diffractometer equipped with CuKα (40 kV, 20 mA) over the range of 0.6 to 8.0° with a step of 0.02 and a contact time of 5 s and transmission electron microscopy (TEM) in a JEOL 3010 electron microscope operating at 300 kV (Cs; 0.6 mm, resolution 1.7 Å). All TEM images were recorded employing a CCD camera (MultiScan model 794, Gatan, 1024 × 1024 pixels size 24 μm × 24 μm) using low-dose condition.

The textural properties of samples were determined by N_2 porosimetry. The N_2 adsorption/desorption analyses were carried out at −196 °C on a Micromeritics ASAP2020 analyzer (Micromeritics Co., Norcross, USA). In all cases, 50−70 mg of material was degassed at 90 °C for 24 h under a vacuum lower than 0.3 kPa before the analysis. The surface area was determined using the Brunauer−Emmett−Teller (BET) method.[21] The total pore volume was estimated from the amount adsorbed at a relative pressure of 0.97. The estimation of microporous and mesoporous fractions to the total pore volume was performed by the *t*-plot method.[22] The average mesopore size (D_P) was obtained from the maximum of the pore size distribution calculated from the adsorption branch of the isotherm by means of the Barrett−Joyner−Halenda (BJH) method.[23] The wall thickness (t_{wall}) was calculated from N_2 adsorption and XRD data as previously reported.[24] To assess the possible existence of micropores (pore diameter <2 nm) in samples, the *t*-plot method was employed, which allowed the estimation of the microporous fraction contribution ($V_{\mu P}$) to the total pore volume. The wall thicknesses (t_{wall}) between adjacent mesopores were calculated from the expression $t_{wall} = a_0 - D_P$, where a_0 is the unit cell parameter calculated from the d_{10} value of XRD using the expression $a_0 = d_{10} \cdot 2/\sqrt{3}$.[24]

The existence of functional groups and their chemical nature were studied by FTIR and XPS in a Thermo Nicolet Nexus spectrometer equipped with a Goldengate attenuated total reflectance (ATR) device and VG Escalab 200R electron spectrometer provided with $MgK\alpha_1$ X-ray ($hv = 1254.6$ eV, 1 eV = 1.6302×10^{-19} J) 120 W source, and a hemispherical electron analyzer, respectively.

XPS has been performed to identify the surface groups, the chemical state of the atoms, and the relative abundance in the different synthesized samples. The samples were deposited as a thin film on double-sided adhesive tape and then mounted on a sample rod, placed in a pretreatment chamber, and degassed at ambient temperature under a residual pressure of 10^{-5} mbar for 1 h prior to being transferred to the analysis chamber. Before the spectra were recorded, the samples were maintained in the analysis chamber under a pressure ca. 2×10^{-9} mbar for 2 h. The area under analysis was around 2.4 mm^2 and the pass energy of the analyzer was set at 20 eV, for which the resolution measured by the full width at half-maximum (fwhm) of the $Au4f_{7/2}$ core level was 0.86 eV. Charging effects were corrected by calibrating spectra to the binding energy of Si2p peak at 103 eV. This reference gave binding energy values with an accuracy of ±0.1 eV. Data processing was performed with the XPS peak software; the spectra were decomposed with the least-squares fitting routine provided with this software using Gauss/Lorentz (90/10) functions and after subtracting a Shirley background. Atomic fractions were calculated using peak areas normalized on the basis of sensitivity factors. Atomic ratios were computed from the intensity ratios normalized by atomic sensitivity factors.[25]

(19) Smoluchowski, M. V. Elektrische Endosmose und Stromungsstrome. In *Handbuch der Electrizitat und des Magnetismus*; Barth: Leipzig, Germany, 1921.
(20) Zhao, D.; Feng, J. P.; Huo, Q.; Melosh, N.; Fredrickson, G. H.; Chmelka, B. F.; Stucky, G. D. *Science* **1998**, *279*, 548.
(21) Brunauer, S.; Emmett, P. H.; Teller, E. *J. Am. Chem. Soc.* **1938**, *60*, 309.
(22) Gregg, S. J.; Sing, K. S. W. *Adsorption, Surface Area and Porosity*, 2nd ed.; Academic Press: New York, 1982.
(23) Barrett, E. P.; Joyner, L. G.; Halenda, P. H. *J. Am. Chem. Soc.* **1951**, *73*, 373.
(24) Kruk, M.; Jaroniec, M.; Sayari, A. *Chem. Mater.* **1999**, *11*, 492.
(25) Wagner, C. D.; Davis, L. E.; Zeller, M. V.; Taylor, J. A.; Raymond, R. H.; Gale, L. H. *Surf. Interface Anal.* **1981**, *3*, 211.

Besides, quantitative determination of functional groups was also carried out by CHNS elemental chemical analysis in a Perkin-Elmer 2400 CHNS thermo analyzer. The loading level of NH_2 and the carbon content sourced from APTES were calculated by the nitrogen content of the analytic results, and the loading level of COOH was calculated by the residual content taking into account the remaining surfactant amount calculated by XPS analyses.

The determination of the residual surfactant amount in samples was performed by thermal analyses (TG and DTA). Measurements were carried out under a dynamic air atmosphere between 30 and 950 °C (flow rate of 50 mL/min with a heating rate of 10 °C/min) using a Perkin-Elmer Diamond analyzer.

To confirm the cross-linking degree and amount of silanol groups in the synthesized materials ^{29}Si nuclear magnetic resonance (NMR) analyses was performed in a Bruker AV-400-WB spectrometer operating at 79.49 MHz for ^{29}Si. The ^{29}Si was recorded by magic angle spinning (MAS) at 12 kHz. Solid samples were analyzed in a 4-mm zirconia rotor. Chemical shifts (δ) of ^{29}Si were externally referred to 3-trimethylsilyl-1-propanesulfonic acid sodium salt (DDS) at $\delta = 0.0$ ppm. The ^{29}Si NMR spectra were recorded with a 4.5-μs wide pulse, a contact time of 3.5 ms, and a recycle delay of 5 s. Typically, 15000 scans were collected. The population of silanol groups per mol of silica has been calculated from the relative population of silanol and geminal species, and divided by the weight per mol of silica materials (eq 1), as previously reported.[26] The weight is derived from the relative populations and effective molecular weights (EMW) of the silanol, geminal, and siloxane species. The effective molecular weight of each species (EMW_Q) is defined as the sum of the molecular weight of the atoms contributing to each species, with the oxygen atoms in the siloxane bridges (Si−O−Si) that connect the species counted by half. The equation is

$$[\mathrm{SiOH}] = \frac{(2 \times \%\mathrm{Q}^2) + \%\mathrm{Q}^3}{(\%\mathrm{Q}^i \times \mathrm{EMW_Q})} \quad (1)$$

where [SiOH] is the silanol group concentration in mol/g and $\%Q^i$ is the relative population of species Q^i (Q^2, Q^3, and Q^4).

Zeta-potential (ζ) measurements were performed in a Zetasizer Nano Series instrument coupled to a MPT-2 multipurpose titrator from Malvern. ζ-potential can be described by Smoluchowski's equation.[27] Ten milligrams of each powdered sample mesoporous was added to 10 mL of KCl 10 mM (used as the supporting electrolyte); the pH was adjusted by adding appropriate volumes of 0.10 M HCl or 0.10 M KOH solutions.

In vitro Assay: Nonspecific STI Adhesion on Functionalized SBA-15 Structures. Soybean trypsin inhibitor (STI, Sigma-Aldrich) adsorption tests were performed by soaking the powdered materials in a sodium acetate buffer solution (25 mM) at pH 5.5 under static conditions at room temperature. STI was chosen as model because it is a small protein (ca. 30 kDa) and its isoelectric point (IEP = 4.6) is very close to those of fibrinogen and the main human plasma proteins (4.7−5.1), which are widely used in nonfouling assays.[28,29] Briefly, 50 mg of the each mesoporous materials were soaked in 1.3 mg/mL of STI at pH = 5.5 during 24 h. Subsequently, the samples were filtered, gently washed with protein-free buffer solution, and dried at room temperature. The determination of the STI adsorbed to the different mesoporous materials was carried out by CHNS elemental chemical analysis and TG/DTA analyses. The experiment was performed in duplicate and the protein adsorption data are expressed in mean ± standard deviation.

Results and Discussion

Doubly functionalized SBA-15 type mesoporous material containing amine and carboxylic groups, noted as $SBA15_{APTES/CES}$, has been synthesized by co-condensation route using 3-aminopropyltriethoxysilane (APTES) together with carboxyethylsilanetriol sodium salt (CES) using the molar compositions displayed in Table 1. For comparative purposes, SBA-15 monofunctionalized with similar molar ratios of amine groups ($SBA15_{APTES}$) and carboxylic groups ($SBA15_{CES}$) were also synthesized (Table 1).

Structural characterization by XRD and TEM reveals that all synthesized samples exhibit ordered mesoporous arrangements typical of SBA-15 structure (Figure 1A and Figure 2).[20] XRD patterns at small angles corresponding to the synthesized samples show a typical profile of 2D-hexagonal structure with *p6mm* plain group in which the well resolved peaks at 1:31/2:2 *d*-spacing ratios can be indexed as 10, 11, and 20 reflections, respectively, of a hexagonal structure similar to that of SBA-15 (Figure 1A). TEM images, taken with the electron beam perpendicular to the mesochannels, indicate that all samples display an ordered mesoporous arrangement with *p6mm* plane group (Figure 2).[30] N_2 adsorption isotherms (Figure 1B) can be identified as type IV isotherms according to the IUPAC classification, which are typical for mesoporous solids.[22] The presence of H1 type hysteresis loops in the mesopore range indicates the existence of open-ended cylindrical mesopores with narrow pore size distributions, which are characteristic of SBA-15 mesoporous matrices. The main textural features derived from the appropriate treatment of N_2 adsorption and XRD data are summarized in Table 2. Textural characterization by N_2 adsorption shows that $SBA15_{APTES/CES}$ material exhibits a specific area of 323 m^2/g and a pore volume of 0.50 cm^3/g, which are almost half of those corresponding to pure SBA-15. The pore diameter also experiences a slight decrease from 8.0 nm for pure silica SBA-15 to 7.1 nm for $SBA15_{APTES/CES}$ sample (Figure 1B and Table 2). This decrease in the textural properties of functionalized materials is in agreement with the appropriate functionalization of mesoporous silica.

Figure 3 shows FTIR spectra corresponding to all synthesized samples. As it can be seen, all spectra show a broad band centered at 3470−3450 cm^{-1}, corresponding to the overlapping of the O−H stretching bands of hydrogen-bonded water molecules (H−O−H) and SiO−H stretching of surface silanols hydrogen bonded

(26) Wouters, B. H.; Chen, T.; Dewilde, M.; Grobet, P. J. *Microporous Mesoporous Mater*. **2001**, *44*, 453.
(27) Hunter, R. J. *Zeta Potential in Colloid Science*; Academic Press: New York, 1981.
(28) Anson, M. L.; Anfirger, C. B. *Advances in Proteins Chemistry*; Vol *10*; Academic Press Int.: New York, 1957.
(29) Harden, V. P.; Harris, J. O. *J. Bacteriol*. **1953**, *65*, 198.
(30) Che, S. N.; Lund, K.; Tatsumi, T.; Iijima, S.; Joo, S. H.; Ryoo, R.; Terasaki, O. *Angew. Chem., Int. Ed*. **2003**, *42*, 2182.

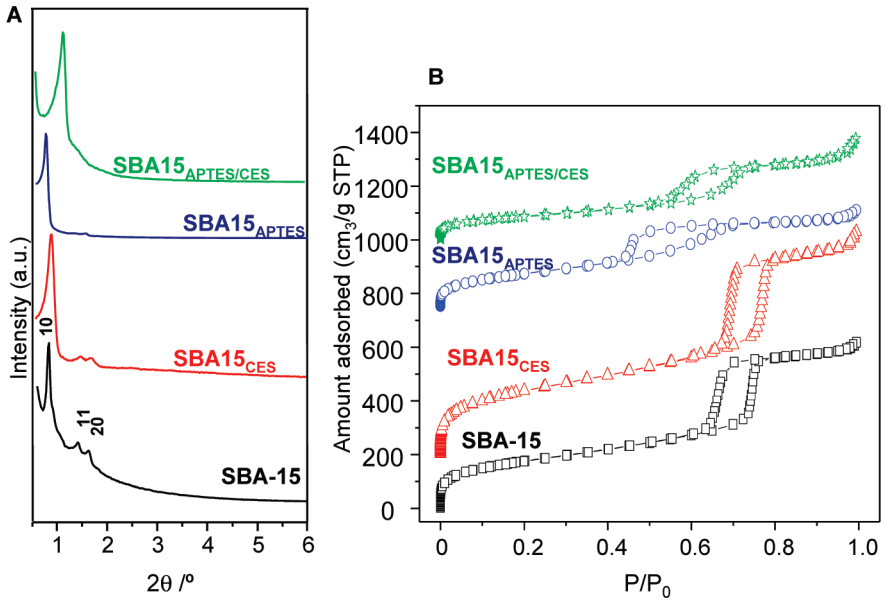

Figure 1. (A) X-ray diffraction patterns and (B) N_2 adsorption isotherms of the different mesoporous samples.

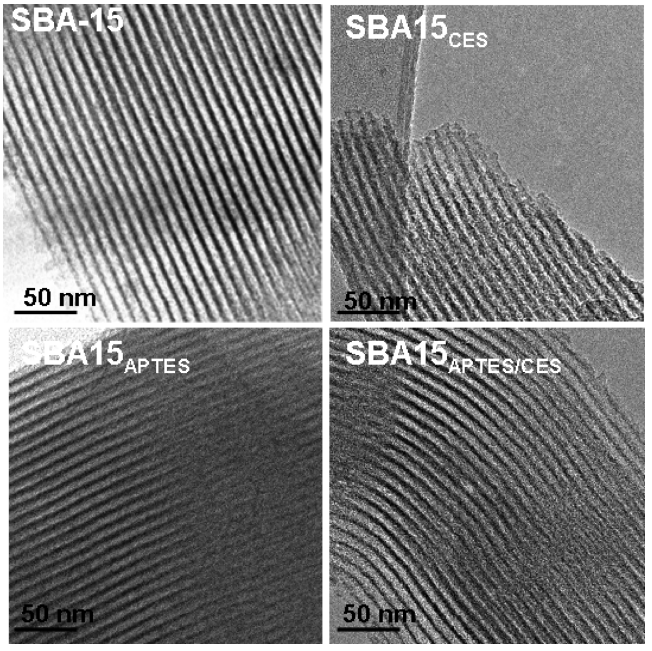

Figure 2. TEM images corresponding to SBA-15, $SBA15_{APTES}$, $SBA15_{CES}$, and $SBA15_{APTES/CES}$ samples.

to molecular water (SiO−H···H_2O). Furthermore, the Si−O in-plane stretching vibrations of the silanol Si−OH groups appear at 960 cm^{-1}. The intense silicon−oxygen covalent bond vibrations appear mainly in the 1100−1000 cm^{-1} range, revealing the existence of a dense silica network, where oxygen atoms play the role of bridges between two silicon sites. Furthermore, the symmetric stretching vibrations of Si−O−Si appear at 800 cm^{-1}, while its bending mode appears at 469−467 cm^{-1}.[31] The low energy band at 560 cm^{-1} is assigned to Si−O stretching of the SiO_2 network defects.[32] In addition, several bands in the 2980−2850 cm^{-1} range, assigned to the C−H symmetric and antisymmetric stretching vibrations of $-CH_2-$ groups in the block copolymer, are also distensible. Note that the intensity of these bands is larger for functionalized samples, which is indicative that there is also a contribution of propyl and ethyl changes of functionalization agents; APTES and CES, respectively.

FTIR spectra of samples functionalized with APTES, $SBA15_{APTES}$ and $SBA15_{APTES/CES}$ samples, display bands at 3344 and 1590 cm^{-1} corresponding to stretching and deformation NH frequencies, respectively, and bands at 3100 and 1480 cm^{-1} corresponding to stretching and deformation $-NH_3^+$ frequencies, respectively.

On the other hand the samples functionalized with CES groups ($SBA15_{CES}$ and $SBA15_{APTES/CES}$ samples) display bands at 1620 and 1400 cm^{-1}, which are typical of the antisymmetric and symmetric frequencies of ionic carbonyl (COO^-). Moreover, only in the case of $SBA15_{CES}$ a band at 1754 cm^{-1} corresponding to carboxylic acid group (COOH) also appears.

In addition, FTIR analyses reveal that $SBA15_{APTES/CES}$ sample exhibit a zwitterionic nature due to presence of NH_3^+ and COO^- groups, as it is demonstrated by XPS analyses. Moreover, all carboxylic groups are presented in its ionic form, i.e., COO^- as it has been confirmed by FTIR because of the absence of bands belonging to −COOH carboxylic acid group in the 1754−1720 cm^{-1} range. Furthermore, $SBA15_{APTES}$ sample exhibits $-NH_2$ and $-NH_3^+$ species, respectively.

XPS of surface groups was undertaken with the purpose to identify the surface groups, the chemical state of the atoms, and their relative abundance in the functionalized SBA-15 samples. All samples showed binding energies of O1s and Si2p core-levels at 532.9 and 103.4 eV, respectively, which are characteristic of silica-based materials (Table 3). In addition to O1s and Si2p emissions, the C1s and N1s

(31) Brinker, C. J.; Scherer, G. W. *Sol−Gel Science: The Physics and Chemistry of Sol−Gel Processing*; Academic Press: San Diego, CA; 1990. p 617.
(32) Al-Oweini, R; El-Rossy, H. *J. Mol. Struct.* **2009**, *919*, 140.

Table 2. Characteristics of the Materials Synthesized in This Work Obtained by N_2 Adsorption, XRD, Elemental Analysis, ^{29}Si Solid State NMRm and ζ-Potential Measurements[a]

sample	S_{BET} (m^2/g)	V_T (cm^3/g)	$V_{\mu P}$ (cm^3/g)	D_P (nm)	a_0 (nm)	t_{wall} (nm)	NH_2/nm^2	COOH/nm^2	SiOH/nm^2	IEP
SBA-15	639	0.92	0.017	8.0	12.6	4.6	-	-	6.6	2.5 ± 0.7
$SBA15_{APTES}$	460	0.52	~0	6.0	11.1	5.1	2.7	-	11.8	5.2 ± 0.4
$SBA15_{CES}$	867	1.2	~0	9.3	12.4	3.1	-	0.9	6.1	1.6 ± 0.6
$SBA15_{APTES/CES}$	323	0.50	~0	7.1	9.6	2.5	2.6	0.9	13.3	5.5 ± 0.3

[a] S_{BET} is the surface area determined by using the BET method between the relative pressures (P/P_0) 0.05−0.25. V_P and $V_{\mu P}$ are, respectively, the total pore volume and micropore volume obtained using the *t*-plot method. The total pore volume was estimated from the amount of N_2 adsorbed at a relative pressure of 0.97. D_P is the pore diameter calculated by means of the BJH method from the adsorption branch of the isotherm. a_0 is the unit cell parameter calculated by XRD, being $a_0 = 2/\sqrt{3}d_{10}$. t_{wall} is the wall thickness calculated using the equation $t_{wall} = a_0 - D_P$.[24] The number of $-NH_2$ and −COOH groups have been determined by elemental analysis. The number of silanol groups (SiOH) has been determined by single pulse ^{29}Si-NMR spectrometry, as described in the experimental section. IEP point is the isoelectric point of samples determined by ζ-potential measurements.

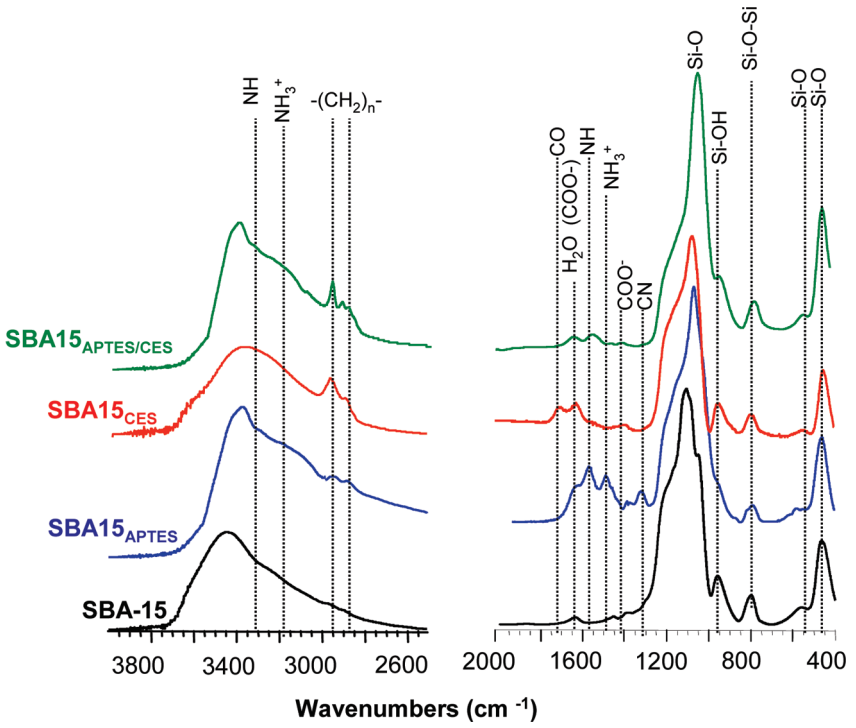

Figure 3. FTIR spectra of SBA-15, $SBA15_{APTES}$, $SBA15_{CES}$, and $SBA15_{APTES/CES}$ samples evidencing incorporated different functional groups.

spectra were recorded for all samples. In the case of $SBA-15_{APTES/CES}$ sample the C1s line profile was fitted to three components at 284.9, 286.8, and 288.6 eV (Figure 4, Table 3). The component at 284.9 eV is associated with CC/CH bonds of the alkyl chains of APTES; CES and small fraction of surfactant[33] and the component at 286.6 eV can be attributed to C−O moieties of remaining surfactant.[34] The component located at 288.6, which represents 10% of the total area of the peaks, is characteristic of COO functional groups attached to SBA-15 surface,[32,33] which would be fully deprotonated carboxylic groups ($-COO^-$) according to FTIR results. The high resolution N1s line profile was rather asymmetrical displaying broadening in the high binding energy side, suggesting that more than one component is present. Indeed, the N1s peak was satisfactorily fitted to two components at binding energies of 400.9 and 402.9 eV (Figure 4, Table 3). The peak at 400.9 eV is usually assigned to $-NH_2$ groups whereas that at 402.9 eV is often considered the response of protonated $-NH_3^+$ moieties,[35,36] which is in good agreement with the results derived from FTIR. From peak areas and atomic sensitivity factors, the atomic surface proportion was determined. According to this calculation, a total C-atom surface proportion of 10.2% was obtained whereas total N-atom concentration was 2.5. By taking into account the fraction of C-atoms belonging to COO^- species and that of N-atoms present in $-NH_3^+$ moiety, a value of 1.04 was calculated for the $-NH_3^+/COO^-$ atomic ratio (Table 3). This value fit with the theoretical value of 1 expected for the formation of zwitterion species on the SBA-15 surface.

N1s XPS spectrum of $SBA15_{APTES}$ sample reveals the presence of NH_2 and NH_3^+ species (Table 3), in agreement

(33) Boehm, H. P. *Carbon* **2002**, *40*, 145.
(34) Barroso-Bujans, F.; Fierro, J. L. G.; Rojas, S.; Sánchez-Cortés, S.; Arroyo, M.; López-Manchado, M. A. *Carbon* **2007**, *45*, 1669.
(35) Zhang, F.; Srinivasan, M. P. *Langmuir* **2004**, *20*, 2309.
(36) An, Y.; Chen, M.; Xue, Q.; Lin, W. *J. Colloid Interface Sci.* **2007**, *311*, 507.

Table 3. Binding Energies (eV) and Surface Composition of SBA-15, $SBA15_{APTES}$, $SBA15_{CES}$, and $SBA15_{APTES/CES}$ Samples (In Parentheses Are Peak Percentages)

sample	Si2p	N1s	C1s	O1s	N %at	C %at
SBA-15	103.4	-	284.9 (21) 286.5 (34) 288.6 (45)	532.9	-	-
$SBA15_{APTES}$	102.1	399.3 (64) 401.1 (36)	284.9 (78) 286.5 (22)	531.6	2.9	9.1
$SBA15_{CES}$	103.4	400.1 (50) 402.8 (50)	284.9 (49) 286.6 (43) 288.6 (8)	532.9	-	8.3
$SBA15_{APTES/CES}$	103.4	400.9 (58) 402.9 (42)	284.9 (30) 286.8 (60) 288.6 (10)	532.9	2.5	10.2

with FTIR results. This likely occurs on −SiOH groups with slightly acidic character. This is in agreement with the absence of line at ca. 199 eV where Cl2p signal would appear. Unfortunately, spectral resolution is not high enough to see any small shoulder overlapping the strong Si2p signal originated by Si−O bond of the SBA-15 lattice. In addition, the C1s line profile in XPS spectrum of $SBA15_{CES}$ sample evidences the presence of COO functional groups. Quantitative evaluation reveals that surface concentration of COOH groups is 2.1 per 100 Si surface atoms.

Quantitative determination of functional groups was also carried out by CHNS chemical elemental analysis, as previously described in the Materials and Methods section. The analytical results show that the loading amount of NH_2 and COOH organic groups was 2.6 and 0.9 groups per nm^2, respectively, for the $SBA15_{APTES/CES}$ sample. On the other hand, $SBA15_{APTES}$ and $SBA15_{CES}$ samples exhibited a monofunctionalization degree of 2.7 NH_2 groups per nm^2 and 0.9 COOH groups per nm^2, respectively (Table 2).

Furthermore, the amount of residual surfactant in all samples after being submitted to corresponding solvent extractions was calculated by TG/DTA analysis and did not exceed 5% in all cases, in agreement with XPS results.

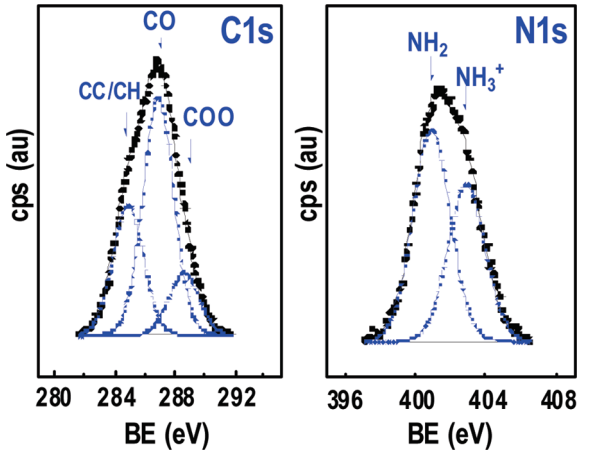

Figure 4. C1s (left) and N1s (right) core-level spectra of $SBA15_{APTES/CES}$ sample obtained from XPS.

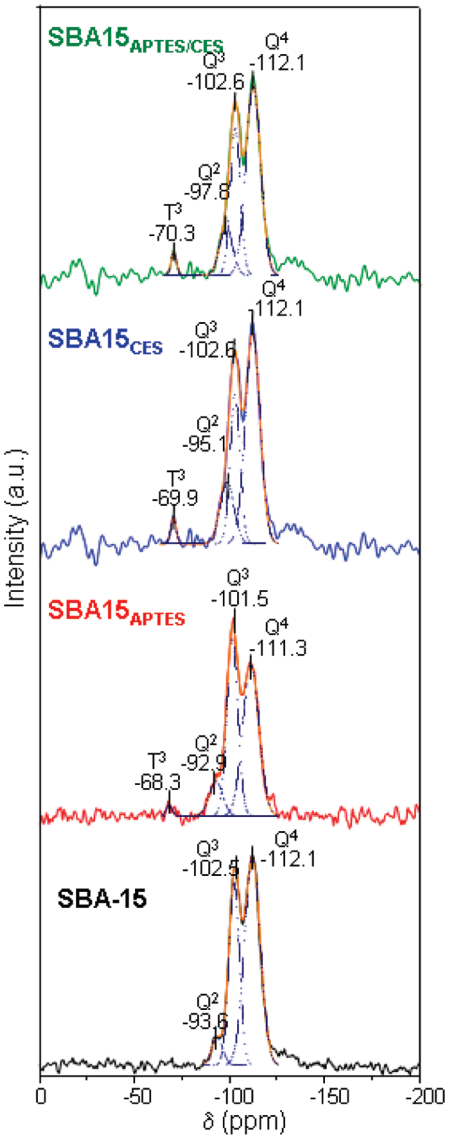

Figure 5. ^{29}Si MAS NMR spectra of the different mesoporous samples.

Further analysis of samples by ^{29}Si NMR was performed to assess the chemical grafting of alkoxysilanes to the silica network. In all the spectra, the resonances at ca. −93, −102, and −112 ppm represent $Q^2[Si(OSi)_2(OX)_2]$, $Q^3[Si(OSi)_3(OX)]$, and $Q^4[Si(OSi)_4]$ silicon sites, respectively (X = H, C) (Figure 5). The populations of these silicon environments were calculated using the integrated intensities of the ^{29}Si NMR spectra and are listed in Table 4. No significant changes are observed in the $Q^2/Q^3/Q^4$ relative populations in all samples. The presence of signals attributable to T^n units $[R\text{-}Si(OSi)_n(OX)_{3-n}]$ (X = H,C) are indicative of the organosilane groups in the materials. The presence of T^3 signals in the three functionalized samples $[R\text{-}Si(OSi)_3]$ functionalities in the NMR spectra at ca. −70 ppm confirms the existence of covalent linkages between the silica surface and the organic groups.

Once the chemical nature of powdered samples was evaluated, their behavior in aqueous media was investigated by carrying out ζ-potential measurements. The IEPs of

Table 4. Peak Area (%) and Standard Deviation of the T″ and Q″ Units on the Basis of Deconvolution of ^{29}Si MAS NMR Spectra of the Different Mesoporous Samples

sample	T^3	Q^2	Q^3	Q^4
SBA-15	-	5.6 ± 0.2	34.9 ± 0.2	59.5 ± 0.2
$SBA15_{APTES}$	1.4 ± 0.1	9.4 ± 0.2	39.4 ± 0.4	49.8 ± 0.2
$SBA15_{CES}$	2.5 ± 0.1	15.5 ± 2.7	26.3 ± 4.6	55.7 ± 0.6
$SBA15_{APTES/CES}$	2.5 ± 0.1	14.1 ± 2.5	27.7 ± 3.5	55.7 ± 0.2

amine-containing samples, $SBA15_{APTES}$ and $SBA15_{APTES/CES}$, were 5.2 and 5.5, respectively (Figure 6). The IEP values are quite close, which could be explained by the presence of a similar number of amine groups (ca. 2.6 per nm^2) in the surfaces of both samples. The coexistence of basic amine functions with a relative high number of acidic SiOH groups in these materials synthesized by co-condensation (Table 2 and Figure 5) originates a relatively slight increase in the IEP value in these samples compared to that of pure silica SBA-15 (IEP = 2.5). Moreover, by comparing $SBA15_{APTES}$, without carboxylic groups, and $SBA15_{APTES/CES}$ sample, with ca. of 1.0 COOH groups per nm^2, no significant differences in the IEP values are observed. These results would indicate that the contribution to the IEP regarding the carboxylic groups is too small compared to the large amount of silanol (SiOH) groups (ca. 13 per nm^2). In fact, in $SBA15_{CES}$, which only contains carboxylic groups as functional agent, a slight decrease in the IEP values is observed compared to pure silica SBA-15 (Table 2 and Figure 6).

From ζ-potential results it can be concluded that amino functionalized and bifunctionalized materials exhibit zero surface charges in aqueous media at pH values close to their IEP, i.e., in the 5.2−5.5 range. Therefore, with the aim of evaluating the influence of the zwitterionic nature of $SBA15_{APTES/CES}$ material surface on protein adsorption, an in vitro study of nonspecific protein adhesion was carried out by soaking all synthesized materials in a protein solution at pH 5.5 and 37 °C. Thus, protein adhesion tests were performed in conditions that favor surface−molecule interactions, which is essential to evaluate the fouling or ultralow-fouling properties of these

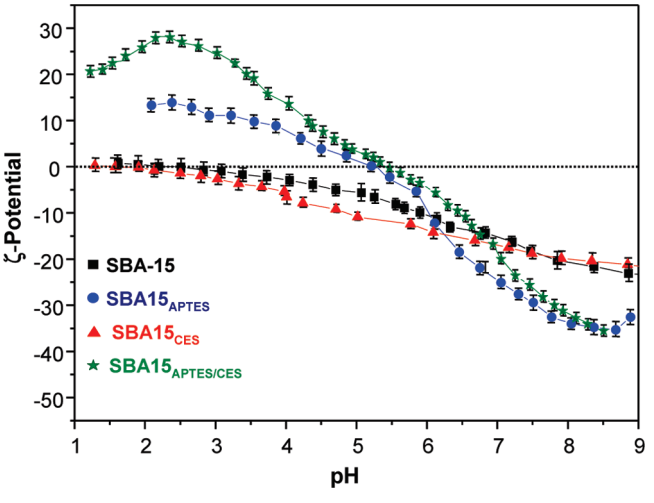

Figure 6. ζ-Potential vs pH plots of the different mesoporous samples.

materials surfaces at the nanometer scale. Taking into account that the mesopore size of the materials synthesized in this work range from 6 to 9 nm, a smaller size protein would be desirable to evaluate the influence of the chemical nature of materials on protein adsorption while avoiding size limitations (see pore diameter for each material in Table 2). The small protein STI, with dimensions of ca. 3 nm × 4 nm × 2 nm, as determined by X-ray crystallography,[37] was chosen as model. Thus, this globular protein could accede to the overall surface area of materials and would be a good choice to evaluate the influence of the chemical nature of materials on protein adsorption. It should be also mentioned that the IEP of STI is ca. 4.6, which is very similar to those of plasma fibrinproteins, bacteria, and *Candida albicans* (4.5−5.5).[28,29] These proteins/microorganisms are usually adsorbed on the surface of biomedical and biotechnological devices, which can provoke some disruptions in the materials efficiency. Therefore, the STI is a proper protein to be used as model during the adhesion tests.

Determination of the amount of protein attached on the surface of each material was performed by CHNS elemental chemical analysis and the derived results are displayed in Figure 7A. The results clearly indicate that the presence of $-NH_3^+$ and $-COO^-$ groups in $SBA15_{APTES/CES}$ sample provides this zwitterionic surface of an ultralow-fouling protein capability with nonspecific STI adsorption of 3.7 ± 0.3 ng/cm^2 (< 5 ng/cm^2).[9] However, $SBA15_{APTES}$ material with a nonspecific STI adsorption of 12.9 ± 0.6 ng/cm^2 does not exhibit such ultralow-fouling capability. These results indicate that the acid character of the carboxylic groups plays a key role in the ultralow-fouling capability of $SBA15_{APTES/CES}$ zwitterionic matrices. It should be also highlighted that $SBA15_{CES}$ and $SBA15_{APTES}$ monofuncionalized samples exhibit higher nonspecific STI adsorption than pure silica SBA-15 due to the presence of functional groups in the former able to electrostatically interact with the functional groups of the protein (Figure 7B). The different behavior of $SBA15_{APTES/CES}$ sample could be explained by the presence of $-NH_3^+$ and $-COO^-$ groups, as confirmed by XPS and FTIR analyses. The existence of both these groups with an overall neutral charge originates a zwitterionic surface that would resist nonspecific protein adsorption via hydration layer bound through solvation of the charged terminal groups in addition to hydrogen bonding. Thus, the water molecules above the zwitterionic surface would create a strong repulsive force on the protein as it approaches the surface, which is in agreement with previous reports for ultralow-fouling materials.[2,38,39]

Conclusions

The design, synthesis, and characterization of novel nanostructured mesoporous ceramics featuring zwitterionic

(37) Hwang, D. L.; Foard, D. E.; Wei., C. H. *J. Biol. Chem.* **1977**, *252*, 1099.
(38) He, Y.; Hower, J.; Chen, S.; Bernards, M. T.; Chang, Y.; Jiang, S. *Langmuir* **2008**, *24*, 10358.

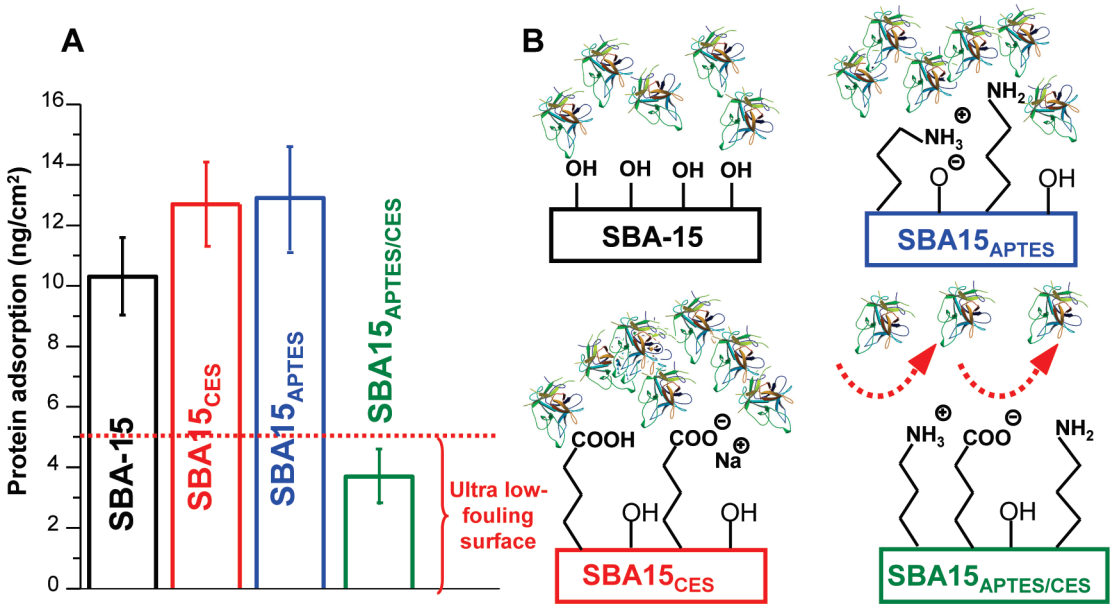

Figure 7. (A) Histogram displaying the amount of STI adsorbed per surface of each material after protein adsorption test by soaking them in a 25 mM acetic/acetate buffered at pH 5.5. The dotted line represents the nonspecific protein adsorption level (< 5 ng/cm^2) below which surfaces are commonly accepted as ultralow-fouling. (B) Scheme displaying the surfaces of different materials synthesized in this work and their fouling and nonfouling behavior at pH. 5.5 toward STI adsorption depending on their chemical nature.

surfaces with high resistance to nonspecific protein adsorption have been performed in this work. The co-condensation route has been employed to bifunctionalize SBA-15 with amine and carboxylic acid groups. The functionalization process following the co-condensation route does not affect the mesostructural order of SBA-15, originating mesoporous matrices with outstanding features suitable for purposes that require host matrices with relatively large mesopores, surface areas, and volumes. It should be also remarked that these materials combine an ultralow-fouling background with the presence of reactive $-$COOH and $-NH_2$ groups able to act as coupling sites to covalently immobilize recognition elements for specific uses. This novel generation of ultralow-fouling ceramics has great potential for applications in catalysis, sensing, biotechnology, and biomedicine.

Acknowledgment. We thank the following for funding this work: the Spanish CICYT through projects MAT2008-00736 and the Comunidad Autónoma de Madrid via the S2009MAT-1472 program grant. We also thank Fernando Conde (CAI X-ray Diffraction), CAI Elemental analysis, CAI NMR, CAI Electron Microscopy of Universidad Complutense de Madrid.

(39) Chen, S.; Zhen, J.; Li, L.; Jiang, S. *J. Am. Chem. Soc.* **2005**, *127*, 14473.